# The near ultraviolet photodissociation dynamics of 2- and 3-substituted thiophenols: Geometric vs. electronic structure effects

Barbara Marchetti, Tolga N. V. Karsili, Maicol Cipriani, Christopher S. Hansen, and Michael N. R. Ashfold

Citation: The Journal of Chemical Physics **147**, 013923 (2017); doi: 10.1063/1.4980035
View online: http://dx.doi.org/10.1063/1.4980035
View Table of Contents: http://aip.scitation.org/toc/jcp/147/1
Published by the American Institute of Physics

# The near ultraviolet photodissociation dynamics of 2- and 3-substituted thiophenols: Geometric *vs.* electronic structure effects

Barbara Marchetti,[a] Tolga N. V. Karsili,[b] Maicol Cipriani, Christopher S. Hansen, and Michael N. R. Ashfold[c]
*School of Chemistry, University of Bristol, Bristol BS8 1TS, United Kingdom*

(Received 27 February 2017; accepted 30 March 2017; published online 26 April 2017)

The near ultraviolet spectroscopy and photodissociation dynamics of two families of asymmetrically substituted thiophenols (2- and 3-YPhSH, with Y = F and Me) have been investigated experimentally (by H (Rydberg) atom photofragment translational spectroscopy) and by *ab initio* electronic structure calculations. Photoexcitation in all cases populates the $1^1\pi\pi^*$ and/or $1^1\pi\sigma^*$ excited states and results in S–H bond fission. Analyses of the experimentally obtained total kinetic energy release (TKER) spectra yield the respective parent S–H bond strengths, estimates of $\Delta E(\tilde{A} - \tilde{X})$, the energy splitting between the ground ($\tilde{X}$) and first excited ($\tilde{A}$) states of the resulting 2-(3-)YPhS radicals, and reveal a clear propensity for excitation of the C–S in-plane bending vibration in the radical products. The companion theory highlights roles for both geometric (e.g., steric effects and intramolecular H-bonding) and electronic (i.e., π (resonance) and σ (inductive)) effects in determining the respective parent minimum energy geometries, and the observed substituent and position-dependent trends in S–H bond strength and $\Delta E(\tilde{A} - \tilde{X})$. 2-FPhSH shows some clear spectroscopic and photophysical differences. Intramolecular H-bonding ensures that most 2-FPhSH molecules exist as the *syn* rotamer, for which the electronic structure calculations return a substantial barrier to tunnelling from the photoexcited $1^1\pi\pi^*$ state to the $1^1\pi\sigma^*$ continuum. The $1^1\pi\pi^* \leftarrow S_0$ excitation spectrum of *syn*-2-FPhSH thus exhibits resolved vibronic structure, enabling photolysis studies with a greater parent state selectivity. Structure apparent in the TKER spectrum of the H + 2-FPhS products formed when exciting at the $1^1\pi\pi^* \leftarrow S_0$ origin is interpreted by assuming unintended photoexcitation of an overlapping resonance associated with *syn*-2-FPhSH($v_{33} = 1$) molecules. The present data offer tantalising hints that such out-of-plane motion influences non-adiabatic coupling in the vicinity of a conical intersection (between the $1^1\pi\sigma^*$ and ground state potentials at extended S–H bond lengths) and thus the electronic branching in the eventual radical products.  [http://dx.doi.org/10.1063/1.4980035]

## I. INTRODUCTION

Fragmentation on an $n\sigma^*$ or $\pi\sigma^*$ state potential energy surface (PES) is now recognised as a competitive non-radiative decay path following near ultraviolet (UV) photoexcitation of many heteroaromatic and heteroatom containing aromatic molecules, e.g., azoles, phenols, thiophenols, and their alkylated analogues.[1–7] Such states can be populated directly, when photoexcitation promotes an electron from the highest occupied *n* (lone pair) or π orbital to the σ* orbital. For brevity, we will henceforth use $^1\pi\sigma^*$ as a shorthand descriptor for all such states. $\sigma^* \leftarrow \pi$ absorption cross sections are generally small, however, and in many cases the initial photoexcitation is to a more strongly absorbing (optically "bright") $^1\pi\pi^*$ state. The net outcome can still be similar, however, if there are energetically accessible regions of degeneracy (so called conical intersections (CIs)) between the $^1\pi\pi^*$ and $^1\pi\sigma^*$ PESs. Non-adiabatic coupling in the vicinity of such a CI enables population transfer to the $^1\pi\sigma^*$ state. Whether the $^1\pi\sigma^*$ state is populated directly or indirectly, the typical outcome in a gas phase experiment is fission of the bond along which the σ* orbital is localised.

Such fragmentation dynamics have been demonstrated in phenol[8–23] and thiophenol,[24–30] in a range of substituted phenols[31–36] and thiophenols,[37–39] and in the methylated analogues anisole[40,41] and thioanisole,[42–46] in both the gas and condensed[47–50] phase. The present study focusses on thiophenols and, particularly, how the much-studied S–H bond fission process is affected by asymmetric substitution (i.e., in the 2- and 3-positions) of the aromatic ring. Previous studies[26,28,38] have reported cuts through the diabatic ground ($S_0$), $1^1\pi\pi^*$, and $1^1\pi\sigma^*$ PESs of bare thiophenol (PhSH), as a function of the S–H bond length ($R_{S-H}$), with all atoms constrained to lie in a plane. The $S_0$ and $1^1\pi\pi^*$ PESs are both bound in all nuclear coordinates. The diabatic $1^1\pi\sigma^*$ PES, in contrast, is dissociative with respect to S–H bond extension, crossing the $1^1\pi\pi^*$ and $S_0$ potentials at, respectively, $R_{S-H} \sim 1.45$ Å

[a] Present address: Department of Chemistry, University of Pennsylvania, Philadelphia, PA, USA.
[b] Present address: Department of Chemistry, Temple University, 13th and Norris Streets, Philadelphia, PA 19122, USA.
[c] Author to whom correspondence should be addressed. Electronic mail: mike.ashfold@bristol.ac.uk

 

(henceforth termed CI-1, between the $1^1\pi\pi^*$ and $1^1\pi\sigma^*$ PESs) and $R_{S-H} \sim 2.6$ Å (CI-2, between the $S_0$ and $1^1\pi\sigma^*$ PESs). Nuclear motion at CI-2 controls the eventual branching between the ground ($\tilde{X}$) and first excited ($\tilde{A}$) states of the PhS radicals formed upon S–H bond fission. These states differ by the relative orientation of the singly occupied molecular orbital (SOMO): the SOMO of the $\tilde{X}$ state radical is dominated by the out-of-plane sulfur $3p_x$ orbital, whereas, in the $\tilde{A}$ state, it is the in-plane $3p_y$ orbital.

Near UV photofragment translational spectroscopy (PTS) studies of thiophenol[24–27] show that the H atom products are formed with anisotropic recoil velocity distributions (indicative of dissociation on a timescale that is fast compared to that of parent rotation). The velocity distributions are also bimodal, consistent with the formation of both $\tilde{X}$ and $\tilde{A}$ state PhS radical co-fragments, and structured. The electronic branching and the details of the structure evident in the velocity distributions both vary with photolysis wavelength. Analysis shows that the partner PhS fragments are formed in a limited sub-set of the energetically available vibrational levels. Identification of these levels affords insight into the fragmentation dynamics and also reveals a propensity for activity in ring-localised vibrational motions that can be traced back to parent vibrations induced in the initial photoexcitation step.[26]

The electronic branching in the radical products has also been shown to be influenced by the presence of different Y-substituents in the 4-(*para*-) position. Replacing H by a methyl group (Y = Me) causes minimal perturbation, but the presence of a strong π-electron donating substituent like methoxyl (Y = MeO) leads to an obvious bias in favour of forming $\tilde{A}$ state radical products.[38] Such outcomes are now understood by considering the geometry of the parent 4-YPhSH molecule and, particularly, the orientation of the S–H bond relative to the ring plane (defined by a torsional angle $\phi$) as it evolves on the $1^1\pi\sigma^*$ PES through the configuration space around CI-2. The SH group is a weak π-donor and thus conjugates poorly with the ring-centred π system. In the case of bare PhSH (or 4-MePhSH), this conjugation suffices to ensure a planar ground state equilibrium geometry (i.e., $\phi_{S-H} = 0°$), and this geometric preference is maintained upon vertical excitation to the $1^1\pi\pi^*$ and $1^1\pi\sigma^*$ states. If this persists during the subsequent S–H bond extension, the dissociating molecules are optimally posed for non-adiabatic coupling (i.e., to follow the diabatic path) at CI-2 and the formation of H + PhS($\tilde{X}$) products. Conversely, in 4-MeOPhSH, the ground state minimum energy geometry has $\phi \sim 90°$. Though the $1^1\pi\pi^*$ and $1^1\pi\sigma^*$ excited states are calculated to have planar equilibrium geometries, the topographies of these excited PESs are such that many of the photoexcited 4-MeOPhSH molecules sample the region of CI-2 with non-planar geometries and follow the adiabatic path to H + 4-MeOPhS($\tilde{A}$) products.[38]

Ways in which substituents in other positions on the ring can influence the photofragmentation dynamics have been explored less systematically. Initial investigations of the effects of substituting phenol with a weakly perturbing (and non-hydrogen bonded) group like methyl (Me) in the 2- or 3-position revealed little obvious change in the tunnelling dynamics under CI-1 following photoexcitation to the $1^1\pi\pi^*$ state.[32] However, a later re-analysis suggests that the reduced symmetry caused by such substitution does affect the detailed vibrational energy disposal in the methylphenoxyl radical products.[35] Much more dramatic effects have been identified when introducing a Cl atom in the 2-position in phenol. Now, the presence of the OH–Cl intramolecular hydrogen bond facilitates a new and efficient non-radiative decay from the photoexcited $1^1\pi\pi^*$ state, via a CI with the $S_0$ PES located along a coordinate associated with eventual HCl elimination, the rate of which overwhelms that of the "traditional," tunnelling enabled O–H bond fission.[36]

This article extends such investigations to asymmetrically substituted thiophenols excited at many different near UV wavelengths. Using a combination of experiment and theory, we explore the extent to which the well-documented S–H bond fission dynamics following near UV photoexcitation of PhSH are influenced by the presence of a weakly perturbing (Me group) and an electron donating substituent (an F atom) in both the 2- and 3-positions. The present work complements and extends the recent ion imaging studies of the H and D atom fragments formed following near UV excitation of 2-FPhSH (2-FPhSD) and 2-ClPhSH (2-ClPhSD).[39] It reveals subtle, Y- and position-dependent effects on the S–H bond strength and/or the energy separation between the $\tilde{A}$ and $\tilde{X}$ states radical, $\Delta E(\tilde{A}(v = 0) - \tilde{X}(v = 0))$. These effects are variously attributable to π-donation (when introducing an F substituent), hyperconjugation (in the case of a Me substituent), steric crowding (in the case of 2-substituents), and intramolecular H-bonding (in the specific case of 2-FPhSH).

## II. METHODS

### A. Experimental

The H Rydberg atom (HRA) PTS setup has been detailed previously,[26,51] so only a brief outline of the apparatus and methodology specific to the present study is given here. The samples (3-MePhSH, 3-FPhSH, 2-MePhSH, and 2-FPhSH, all supplied by Sigma Aldrich) are liquids at room temperature and were used without further purification. For orientation purposes, room temperature UV absorption spectra were measured for each sample (as a dilute solution in *n*-hexane), and attempts were made to record jet-cooled, 1+1 resonance multiphoton ionisation (REMPI) spectra of the respective parent molecules in the gas phase at wavelengths around the long wavelength onset revealed by the absorption data.

In the photolysis experiments, the sample of interest was packed in a stainless steel in-line filter positioned before a pulsed valve. The filter housing was heated resistively to boost the sample vapour pressure, which was then diluted in ~700 Torr of Ar and supersonically expanded and skimmed, thereby presenting a collimated beam of the jet-cooled target species within the differentially pumped interaction volume. The jet-cooled sample was crossed by the outputs of three Nd:YAG pumped, frequency doubled pulsed dye lasers. The photolysis laser in this work yielded wavelengths in the range 290-242 nm. (All photolysis wavelengths are reported here as wavelengths in vacuum.) After a short ($\delta t \sim 10$ ns) time delay, H atom photoproducts in the interaction volume were promoted to a Rydberg state with high *n* principal quantum number using

a 1+1′ (121.6 nm (Lyman-α, formed by frequency tripling ~364.7 nm radiation in a phase matched Kr/Ar mixture) + 366 nm) double resonant excitation scheme. Any unintended ions formed in the interaction region were removed using a 50 V $cm^{-1}$ extraction field. Rydberg-tagged H atoms with recoil velocities along the detection axis fly a known distance and are then field ionised upon passing through a grounded mesh and detected by a double microchannel plate detector. H atom time-of-flight (TOF) spectra derived in this way were then converted into total kinetic energy release (TKER) spectra using the following equation:

$$\mathrm{TKER} = \frac{1}{2} m_{\mathrm{H}} \left(1 + \frac{m_{\mathrm{H}}}{m_{\mathrm{R}}}\right) \left(\frac{d}{t}\right)^2, \tag{1}$$

where $m_{\mathrm{H}}$ and $m_{\mathrm{R}}$ are, respectively, the masses of the H atom (1.007 94 u) and the assumed radical co-fragment (MePhS = 124.20 u, FPhS = 128.17 u), $d$ is the distance between the interaction volume and the detector, and $t$ is the measured TOF. A $t^{-3}$ Jacobian was used when re-binning the signal intensities as a part of the transformation from TOF to TKER spectra. The polarisation vector of the photolysis laser ($\boldsymbol{\varepsilon}_{\mathrm{phot}}$) in "standard" operation was perpendicular to the TOF axis (i.e., $\boldsymbol{\varepsilon}_{\mathrm{phot}} = 90°$). However, selected spectra were also measured with $\boldsymbol{\varepsilon}_{\mathrm{phot}}$ set at 0° (i.e., parallel) and at 54.7° (i.e., at the magic angle) to the TOF axis in order to check for any anisotropy in the H atom product recoil velocity distribution and its TKER dependence.

### B. Computational methods

Various *ab initio* calculations were undertaken using MOLPRO, version 2010.1.[52] The relative stabilities of the *syn* and *anti* rotamers in the $S_0$ states of these asymmetrically substituted 2-(3-)YPhSH molecules were explored at different levels of theory. First, the relaxed $S_0$ potential was scanned as a function of the C(2)C(1)S–H torsional coordinate ($\phi$), where $\phi = 0°$ defines a planar configuration with the H atom in the SH group pointing toward the side of the ring supporting the Y-substituent. The angle $\phi$ was stepped in 15° increments between $0° \le \phi \le 180°$ and, at each value of $\phi$, the $S_0$ geometry was optimised by allowing all other internal degrees of freedom to relax to their respective minima. These calculations used Møller-Plesset second order perturbation theory (MP2)-coupled to Dunning's augmented correlation consistent basis set of triple-ζ quality: aug-cc-pVTZ, henceforth AVTZ.[53] In order to describe the extensive virtual orbitals of the S atom and any possible Rydberg-valence mixing, an additional tight *d* polarisation function and extra even-tempered *s* and *p* diffuse functions were added to the S atom (henceforth referred to as aug(S)-AVTZ). Vertical excitation energies to the $1^1\pi\pi^*$ and $1^1\pi\sigma^*$ states were then computed at these relaxed $S_0$ geometries along the $\phi$ coordinate using the equation-of-motion coupled cluster singles and doubles (EOM-CCSD) level of theory[54] and a smaller valence double-ζ basis set with, again, extra even-tempered sets of *s* and *p* diffuse functions on S (henceforth termed aug(S)-VTZ).

The $1^1\pi\pi^* \leftarrow S_0$ and $1^1\pi\sigma^* \leftarrow S_0$ vertical excitation energies and oscillator strengths were also computed using complete active space with second order perturbation theory (CASPT2) coupled with the AVDZ basis set for both the *syn*- and *anti*-rotamers of 2-FPhSH, and for the lower energy rotamer of each of 2-MePhSH, 3-MePhSH, and 3-FPhSH, using the MP2 optimised $S_0$ minimum energy geometries in each case. These calculations were based on a complete active space self-consistent field (CASSCF) reference wavefunction that used state averaged orbitals comprising three states of A′ and two states of A″ symmetry. The chosen active space for 2-(3-)MePhSH involved ten electrons distributed in ten orbitals (10/10). Seven of these (the three π and three π* ring-centred orbitals and the $p_x$ orbital centred on the S atom) transform as a″, while the remaining three a′ orbitals account for the σ and σ* orbitals localised around the S–H bond and the virtual 4s Rydberg orbital centred on the S atom. An additional a″ orbital was included for the 2-(3-)FPhSH calculations, to accommodate the $p_x$ orbital of the F atom, resulting in a (12,11) active space. Oscillator strengths, $f_{ij}$, between the initial ($i$; $S_0$) and final ($j$; $1^1\pi\pi^*$ and $1^1\pi\sigma^*$) states were calculated using the following equation:

$$f_{ij} = \frac{2}{3}\left(E_j - E_i\right) \cdot \sum_{\alpha=x,y,z} \left|\mu_{ij}\right|^2_{\alpha}, \tag{2}$$

where the energies ($E_i$ and $E_j$) and transition dipole moments ($\mu_{ij}$) were obtained from a SA5-CASSCF/AVDZ calculation based on the MP2/aug(S)-AVTZ relaxed equilibrium geometry.

Potential energy curves (PECs) along $R_{\mathrm{S-H}}$ were also calculated for the $S_0$, $1^1\pi\pi^*$, and $1^1\pi\sigma^*$ states of each molecule, by stepping $R_{\mathrm{S-H}}$, while, in this case, holding the ring geometry clamped at that of the $S_0$ state equilibrium geometry. We henceforth describe these as rigid-body scans. The relaxed energies of the $S_0$ and $1^1\pi\sigma^*$ states were also calculated at $R_{\mathrm{S-H}}$ = 5.0 Å, at the same level of theory, in order to determine the 2-(3-)YPhS($\tilde{X}$) + H and 2-(3-)YPhS($\tilde{A}$) + H asymptotes, and thus the S–H bond dissociation energy and the energy splitting between the $\tilde{X}$ and $\tilde{A}$ states of the respective 2-(3-)YPhS radicals.

Ground state anharmonic normal mode wavenumbers were computed using density functional theory (DFT)/B3LYP[55] with a Pople 6-311G+(*d*,*p*) basis set,[56] using the Gaussian 09 computational package[57] in order to aid assignment of vibrational levels populated in the 2-(3-)YPhS radical fragments.

## III. RESULTS AND DISCUSSION

### A. Ground state structure

The MP2/aug(S)-AVTZ optimised minimum energy geometries of the $S_0$ states of 2- and 3-YPhSH (Y = Me and F) are displayed in Figure 1, along with calculated PE profiles along $\phi$ for the $S_0$, $1^1\pi\pi^*$, and $1^1\pi\sigma^*$ states of each molecule. The presence of a 2- or 3-substituent creates an inevitable asymmetry, which gives rise to rotamers distinguished by the relative orientation of the SH bond toward (*syn*) or away from (*anti*) the Y substituent.

We first consider the PE profiles of 3-MePhSH and 3-FPhSH shown in Figs. 1(b) and 1(d). Substituents in the 3-position will cause least electronic (or steric) perturbation in a molecule like PhSH, consistent with the present finding that the *syn* and *anti* rotamers are essentially degenerate, and that the energy barrier to their interconversion is only

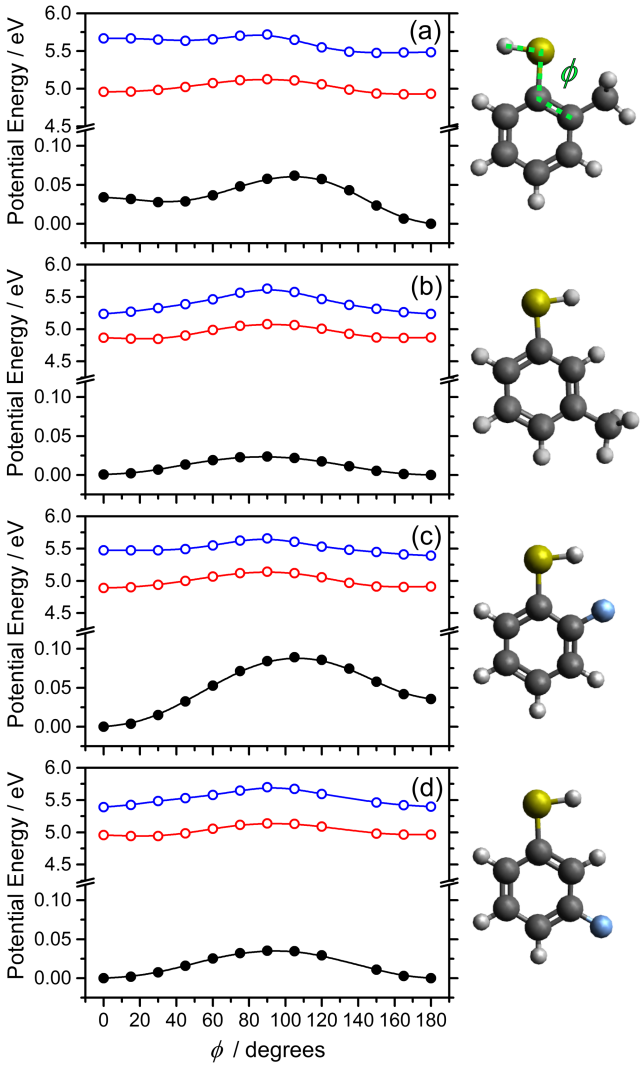


FIG. 1. Potential energy profiles along the $\phi$ coordinate for the $S_0$, $1^1\pi\pi^*$, and $1^1\pi\sigma^*$ states of (a) 2-MePhSH, (b) 3-MePhSH, (c) 2-FPhSH, and (d) 3-FPhSH, together with the respective minimum energy structures. The coordinate describing torsion about the C(2)C(1)SH dihedral is highlighted on the structure shown at the top right.

weakly dependent on the nature of Y. The returned minimum energy geometries of both 3-YPhSH species have all atoms in a common ring plane—as in the corresponding 4-MePhSH and 4-FPhSH analogues.[38] The barrier to *syn* ↔ *anti* rotational isomerism in 3-MePhSH (i.e., a full 180° rotation in $\phi$) is similar to that calculated for 4-MePhSH, reinforcing the view that Me substitution causes minimal perturbation of the electronic properties of PhSH.

The earlier calculations for the torsional potential of 4-FPhSH($S_0$) returned a local minimum at $\phi = 90°$, just ~20 $cm^{-1}$ above the global minimum energy geometry at $\phi = 0°$.[38] As Fig. 1(d) shows, the corresponding potential for 3-FPhSH($S_0$) shows a maximum at $\phi = 90°$; the height of this barrier (~280 $cm^{-1}$) is similar to that found in bare PhSH.[26] The very different PE *vs*. $\phi$ profiles for 3- and 4-FPhSH can be understood by recognising that the SH group, a π-donor, directs electron density to the 2- and 4-positions of the ring and renders the 3-position electrophilic. Substituting an F atom (another π-donor) at the 4-position thus leads to increased electron repulsion within the π-system, which can be relieved by rotating the S–H bond out of the plane—thereby unconjugating the S($3p_x$) orbital and aligning the S–H bond localised σ* orbital with the ring π-system. The 3-position, in contrast, is stabilised by a π-donating substituent. In this case, rotating the SH group out of the plane weakens the π-conjugation, explaining the ~10-times larger torsional barrier height in 3-FPhSH (cf. 4-FPhSH[38]).

The proximity of the Y substituent in the 2-YPhSH molecules can give rise to additional steric and, in the case of 2-FPhSH, intramolecular hydrogen bonding effects. We start by considering 2-MePhSH. The PE *vs* $\phi$ profile (Fig. 1(a)) shows minima associated with both *syn* ($\phi \sim 30°$) and *anti* ($\phi = 180°$) rotamers. The latter is the more stable, reflecting the greater steric interaction at $\phi = 0°$. The PE *vs* $\phi$ profile for 2-FPhSH (Fig. 1(c)) also shows minima at both the *syn* and *anti* geometries, but in this case the *syn* rotamer is the more stable. The switch in relative stabilities (cf. 2-MePhSH) is attributable to the intramolecular hydrogen bond between the thiol H atom and the 2-F substituent when $\phi = 0°$. This stabilising interaction also accounts for the larger barrier to *syn* → *anti* rotational isomerism in 2-FPhSH (Fig. 1(c)) than in 2-MePhSH or either of the 3-YPhSH systems. The present findings for 2-FPhSH accord with the recent study of Han *et al.*,[39] though the energy difference between the *syn* and *anti* rotamers and the height of the barrier to interconversion on the $S_0$ PES are both smaller in the present work. This can be understood since, unlike Han *et al.*,[39] we have allowed the rest of the nuclear framework to relax to its minimum energy geometry when calculating the energy at each value of $\phi$ (i.e., we have calculated the minimum energy path along $\phi$).

## B. Parent molecule spectroscopy

Figure 2 shows near UV absorption spectra for all four parent molecules of current interest recorded in *n*-hexane solution, at room temperature. Figure 2(c) also includes a portion of the jet-cooled REMPI spectrum of 2-FPhSH, from Han *et al.*[39] The long wavelength part of this REMPI spectrum was reproduced in the present study, but no similar sharp structure was measured for the other three species. This comparison suggests a small bathochromic (red-)shift on going from the gas phase to *n*-hexane solution, similar to that found when comparing the near UV absorption spectra of 4-MePhSH in solution in cyclohexane (another weakly interacting solvent) and in the gas phase.[50] Guided by the previous studies of PhSH[26] and the various 4-YPhSH molecules,[38] and the vertical excitation energies and oscillator strengths calculated for the present molecules (Table I), we conclude the following: (i) absorption to the $1^1\pi\pi^*$ state is the dominant contributor at the longest excitation wavelengths, (ii) this absorption is likely to be supplemented by $1^1\pi\sigma^* \leftarrow S_0$ absorption as the excitation wavelength is reduced, and (iii) $2^1\pi\pi^* \leftarrow S_0$ absorption accounts for the more intense absorption at shorter wavelengths (peaking at ~235 nm in all cases).

## C. Photodissociation dynamics

### 1. MePhSH

H atom TOF spectra were recorded following photolysis of both 2- and 3-MePhSH at several wavelengths ($\lambda_{phot}$) in the

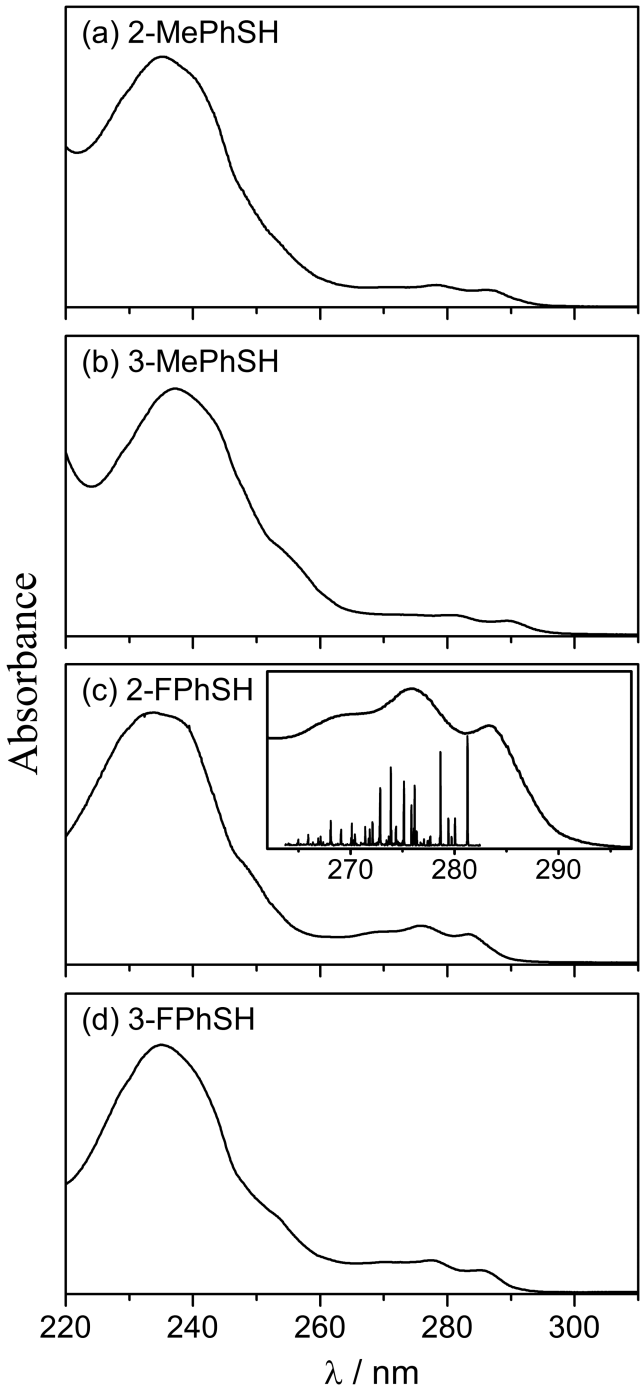


FIG. 2. UV absorption spectra of (a) 2- and (b) 3-MePhSH, and (c) 2- and (d) 3-FPhSH, each recorded in *n*-hexane solution, along with (as an inset in (c)) the jet-cooled REMPI spectrum of 2-FPhSH reported by Han *et al.*[39]

range $290 \geq \lambda_{phot} \geq 250$ nm. In many cases, the signal intensity was clearly sensitive to the orientation of $\boldsymbol{\varepsilon}_{phot}$ relative to the TOF axis. Quantitative studies were challenging, given the difficulty in ensuring no change in the overlap of the three laser beams when varying the polarisation of one (the photolysis beam) by rotating a Fresnel rhomb. Nonetheless, H atom TOF spectra recorded at the very longest photolysis wavelengths for both 2- and 3-MePhSH were clearly more intense when $\theta = 0°$ and we estimate a recoil anisotropy parameter $\beta$ of ~+1. Just a small reduction in $\lambda_{phot}$ (to ≤283 nm in the case of 2-MePhSH) leads to an obvious change in recoil anisotropy; our best estimate of the anisotropy parameter at this wavelength is $\beta \sim -0.3$. Such a behaviour is consistent with previous observations for PhSH and the various 4-YPhSH analogues.[26,38] Excitation at the very longest wavelengths is predominantly to the $1^1\pi\pi^*$ state, which is efficiently predissociated by coupling to the $1^1\pi\sigma^*$ state. The recoil anisotropy is determined by the initial $1^1\pi\pi^* \leftarrow S_0$ excitation, for which the transition dipole moment (TDM) lies in-plane and near parallel to the breaking S–H bond. However, the $1^1\pi\sigma^* \leftarrow S_0$ TDM is directed out-of-plane, near perpendicular to the S–H bond, and the $\lambda_{phot}$-dependent recoil anisotropy can be understood by assuming that direct excitation to the $1^1\pi\sigma^*$ state gains in relative importance upon tuning to shorter $\lambda_{phot}$.

TABLE I. CASPT2/aug(S)-AVTZ calculated vertical excitation energies (in eV), oscillator strengths *f*, and components of the dipole moments for transitions to the $1^1\pi\pi^*$ and $1^1\pi\sigma^*$ states of 3-MePhSH, 3-FPhSH, 2-MePhSH, and 2-FPhSH. The energies in parentheses are the *anti*-2-FPhSH excited state energies referenced to that of the *anti*-2-FPhSH minimum. *yz* defines the molecular plane.

| Molecule transition | Energy (eV) | *f* | Transition dipole moments $\mu_x$ | $\mu_y$ | $\mu_z$ |
|---|---|---|---|---|---|
| *syn*-3-MePhSH | | | | | |
| $1^1\pi\pi^* \leftarrow S_0$ | 4.33 | 0.0016 | 0 | 0.0431 | 0.1106 |
| $1^1\pi\sigma^* \leftarrow S_0$ | 4.96 | 0.0090 | −0.2634 | 0 | 0 |
| *syn*-3-FPhSH | | | | | |
| $1^1\pi\pi^* \leftarrow S_0$ | 4.39 | 0.0043 | 0 | −0.1014 | −0.1651 |
| $1^1\pi\sigma^* \leftarrow S_0$ | 4.99 | 0.0058 | 0.2084 | 0 | 0 |
| *anti*-2-MePhSH | | | | | |
| $1^1\pi\pi^* \leftarrow S_0$ | 4.39 | 0.0011 | 0 | −0.0437 | −0.0891 |
| $1^1\pi\sigma^* \leftarrow S_0$ | 5.10 | 0.0111 | −0.2910 | 0 | 0 |
| *syn*-2-FPhSH | | | | | |
| $1^1\pi\pi^* \leftarrow S_0$ | 4.59 | 0.0042 | 0 | 0.0593 | −0.1750 |
| $1^1\pi\sigma^* \leftarrow S_0$ | 5.37 | 0.0024 | 0.1286 | 0 | 0 |
| *anti*-2-FPhSH | | | | | |
| $1^1\pi\pi^* \leftarrow S_0$ | 4.62 (4.70) | 0.0058 | 0 | −0.0911 | 0.1990 |
| $1^1\pi\sigma^* \leftarrow S_0$ | 5.30 (5.38) | 0.0068 | 0.2234 | 0 | 0 |

Illustrative TKER spectra derived from TOF spectra of H atoms resulting from photolysis of 2- and 3-MePhSH assuming that $m_R = 124.20$ u are displayed in Figures 3 and 4, respectively. As with PhSH and the 4-YPhSH analogues,[26,38] the TKER spectra (particularly those recorded at long $\lambda_{phot}$) show two maxima attributable to the formation of the co-fragment R in its ground ($\tilde{X}$) and first excited ($\tilde{A}$) states. Each of these features contain hints of sub-structure, associated with population of specific vibrational states within each electronic state of the R product. Following past precedent,[38] we assign the fastest peak (i.e., the peak with $TKER_{max}$) in spectra recorded at long $\lambda_{phot}$ to the formation of $\tilde{X}$ state radicals in their zero-point (v = 0) vibrational level and thereby obtain an estimate of the S–H bond dissociation energy,

$$D_0(R-H) = E_{phot} + E_{int}(RH) - TKER_{max} - E_{int}(R), \quad (3)$$

where $E_{phot}$ is the photon energy, $E_{int}(RH)$ is the internal energy (in excess of its zero-point energy) in the parent molecule, and, by virtue of the assumed assignment, the

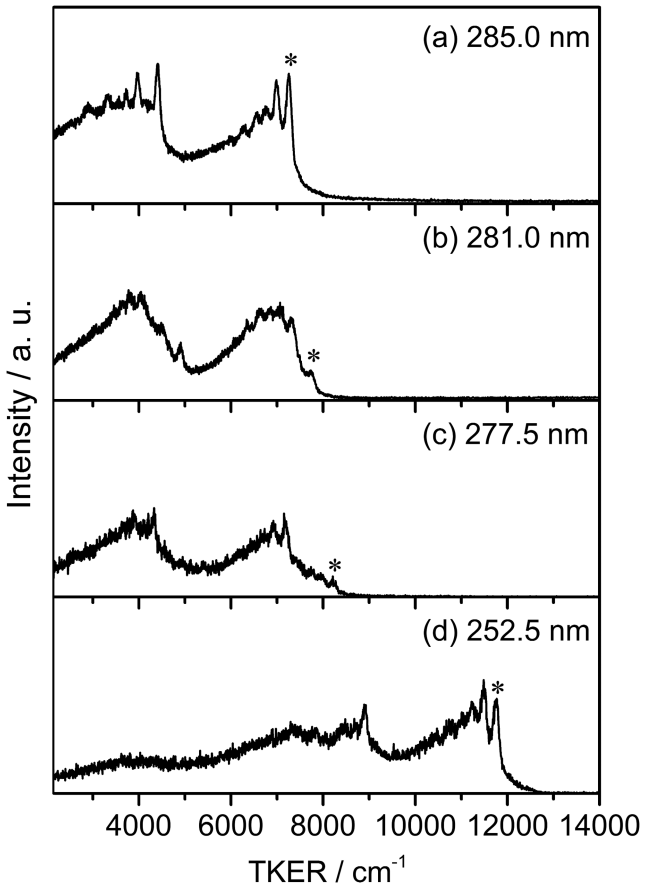


FIG. 3. TKER spectra of the H + 2-MePhS products derived by converting H atom TOF spectra measured following photolysis of 2-MePhSH at $\lambda_{phot}$ = (a) 285.0, (b) 281.0, (c) 277.5, and (d) 252.5 nm. In each spectrum, the $TKER_{max}$ peak attributed to the formation of H + 2-MePhS($\tilde{X}$), v = 0 products is indicated with an asterisk.

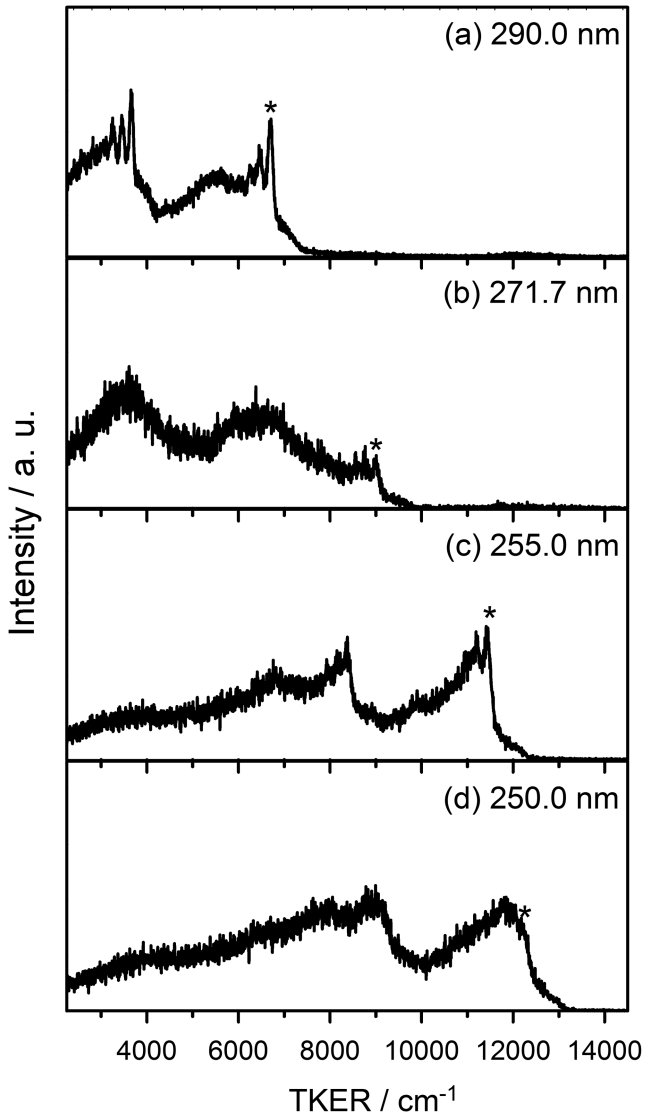


FIG. 4. TKER spectra of the H + 3-MePhS products derived by converting H atom TOF spectra measured following photolysis of 3-MePhSH at $\lambda_{phot}$ = (a) 290.0, (b) 271.7, (c) 255.0, and (d) 250.0 nm. In panels (a)–(c), the asterisk indicates the $TKER_{max}$ peak attributed to the formation of H + 3-MePhS($\tilde{X}$), v = 0 products. The asterisk in (d) indicates the predicted $TKER_{max}$ value for such products.

internal energy of the R fragment, $E_{int}(R) = 0$. Given our use of a jet-cooled sample, $E_{int}(RH)$ is generally considered to be negligible, but proper inclusion of this term will be important in our later analysis of TKER spectra obtained following the long wavelength photolysis of 2-FPhSH.

Table II lists the S–H bond dissociation energies for 2- and 3-MePhSH obtained in this way. The sharpness of the structure in the better-resolved TKER spectra merits comment. In the case of 2-MePhSH (Figure 3), the energy splitting between the *syn* and *anti* rotamers is sufficiently large that the latter will be dominant in our jet-cooled sample. Thus, we associate the derived $D_0$(R–H) value with *anti*-2-MePhSH. The calculated energy splitting between the corresponding conformers in 3-MePhSH is much smaller—less than the full width half maximum of the sharpest features in Figure 4(a). In this case, therefore, the quoted bond strength applies to both rotamers. As Table II shows, the $D_0$(R–H) values determined experimentally for *anti*-2-MePhSH and for 3-MePhSH (both conformers) are, to within experimental uncertainty, the same: 27 820 ± 50 and 27 800 ± 50 $cm^{-1}$, respectively. The CASPT2/aug(S)-AVTZ calculations return slightly lower S–H bond dissociation energies (after zero-point correction), but similarly imply that the Me substituent causes minimal perturbation of the electronic structure.

Armed with the relevant bond strengths, we can recast all TKER spectra for any given parent on a common $E_{int}$ scale. By way of illustration, Figure 5 shows a selection of $E_{int}$ spectra for the 2-MePhS radicals formed by photolysis of *anti*-2-MePhSH at several different $\lambda_{phot}$ values. The trends with decreasing $\lambda_{phot}$ show obvious parallels with previous observations regarding the energy disposal in the $\tilde{X}$ and $\tilde{A}$ state radical products from photolysis of PhSH and the various 4-YPhSH analogues.[26,38] Assigning the first peak in the higher $E_{int}$ feature to 2-MePhS($\tilde{A}$), v = 0 products allows the estimation of the term value of the $\tilde{A}$ state radical, $\Delta E(\tilde{A}(v = 0) - \tilde{X}(v = 0)) = 2850 \pm 50\ cm^{-1}$. A similar analysis of the 3-MePhS data (see Figure S1 in the supplementary material) yields $\Delta E(\tilde{A}(v = 0) - \tilde{X}(v = 0)) = 3015 \pm 50\ cm^{-1}$. As Table II shows, these values are sensibly similar to the reported term values for the $\tilde{A}$ states of PhS[58] and 4-MePhS,[38] and in reasonable accord (both in an absolute and a relative sense) with the *ab initio* predictions. We return to rationalise small differences between these various values in Section III D.

TABLE II. S–H bond dissociation energies ($D_0$(R–H)) and energy separations between the ground ($\tilde{X}$) and first excited ($\tilde{A}$) states of the radical R for the 2- and 3-YPhSH (Y = Me, F) molecules derived in the present work, along with previous data for the corresponding 4-YPhSH species[38] and for PhSH.[26,59] The theoretical $D_0$(R–H)) values were calculated at the CASPT2/aug(S)-AVTZ level with geometry relaxations, and zero-point corrected using normal mode wavenumbers for 2-(3-)YPhSH and 2- (3-) YPhS calculated at the DFT/B3LYP/6-311+G(d,p) level of theory. The experimental $\Delta E(\tilde{A} - \tilde{X})$ values are the estimated v = 0 – v = 0 level separations (i.e., the $T_{00}$ value), whereas the theoretical values have not been corrected for any difference in the zero-point energies of the two states and are thus best regarded as $T_e$ values.

| | $D_0$(R–H) (cm$^{-1}$) | | $\Delta E$ ($\tilde{A} - \tilde{X}$) (cm$^{-1}$) | |
|---|---|---|---|---|
| Molecule | Experimental | Theoretical | Experimental | Theoretical |
| PhSH | 28 030 ± 50 | ... | 3000 ± 7[58] | 2674 |
| 3-MePhSH | 27 800 ± 50 | 25 900 | 3040 ± 50 | 2680 |
| 3-FPhSH | 28 130 ± 50 | 26 110 | 2790 ± 50 | 2490 |
| 2-MePhSH | 27 820 ± 50 | 25 840 (*syn*)<br>26 040 (*anti*) | 2850 ± 50 | 2450 |
| 2-FPhSH | 28 310 ± 50 (*syn*) | 26 410 (*syn*)<br>26 130 (*anti*) | 2780 ± 50 | 2420 |
| 4-MePhSH | 27 430 ± 50 | ... | 3320 ± 50 | 2992 |
| 4-FPhSH | 27 420 ± 50 | ... | 3420 ± 50 | ... |

We now focus attention on the vibrational structure of the 2-MePhS radical revealed in Figure 5. Assignment is guided by reference to the calculated normal mode wavenumbers for the $\tilde{X}$ state radical (listed in Table S1 of the supplementary material), along with an assumption that these also provide a reasonable estimate of the corresponding mode wavenumbers in the $\tilde{A}$ state. All of the $E_{int}$ spectra show short progressions with peak separations of ~260 cm$^{-1}$ and ~490 cm$^{-1}$, consistent with population of radical modes $\nu_{26}$ and $\nu_{24}$ in Herzberg notation[59] ($\nu_{18b}$ and $\nu_{6a}$ in Wilson notation[60]). The nuclear eigenvectors of $\nu_{26}$ and $\nu_{24}$ correspond to in-plane C–S wagging and ring-centred breathing motions, respectively (see Fig. 5). As in the previous PTS studies of photoinduced S–H bond fission in PhSH and 4-YPhSH,[26,38] activity in these modes can be understood in terms of the impulse on the S atom induced by the departing H atom. Moving to shorter $\lambda_{phot}$ (higher $E_{phot}$), the analogous progressions appear shifted to higher $E_{int}$, offset by, e.g., $E_{int}$ ~ 1030 cm$^{-1}$ in the spectrum obtained at $\lambda_{phot}$ = 277.5 nm (Figure 5(d)). This shift matches with a single quantum of radical mode $\nu_{19}$ ($\nu_1$ in Wilson notation). The nuclear eigenvectors for this in-plane ring-breathing motion are also shown in Figure 5. Again, we recognise a clear parallel with the behaviour reported previously in the UV photodissociation of PhSH[26] and various 4-YPhSH species.[38] Activity in such a "spectator" mode (viewed from the perspective of the breaking S–H bond) can be understood on Franck-Condon grounds. $\pi^* \leftarrow \pi$ excitation encourages ring expansion in the photoexcited parent molecule, which then projects onto the eventual 2-MePhS radical. The form of the TKER spectra evolves again on moving to yet a shorter $\lambda_{phot}$ (e.g., 252.5 nm, Fig. 3(d)). The parent absorption data (Figure 2) imply that photoexcitation will now populate the strongly absorbing $2^1\pi\pi^*$ state which we deduce to dissociate by coupling

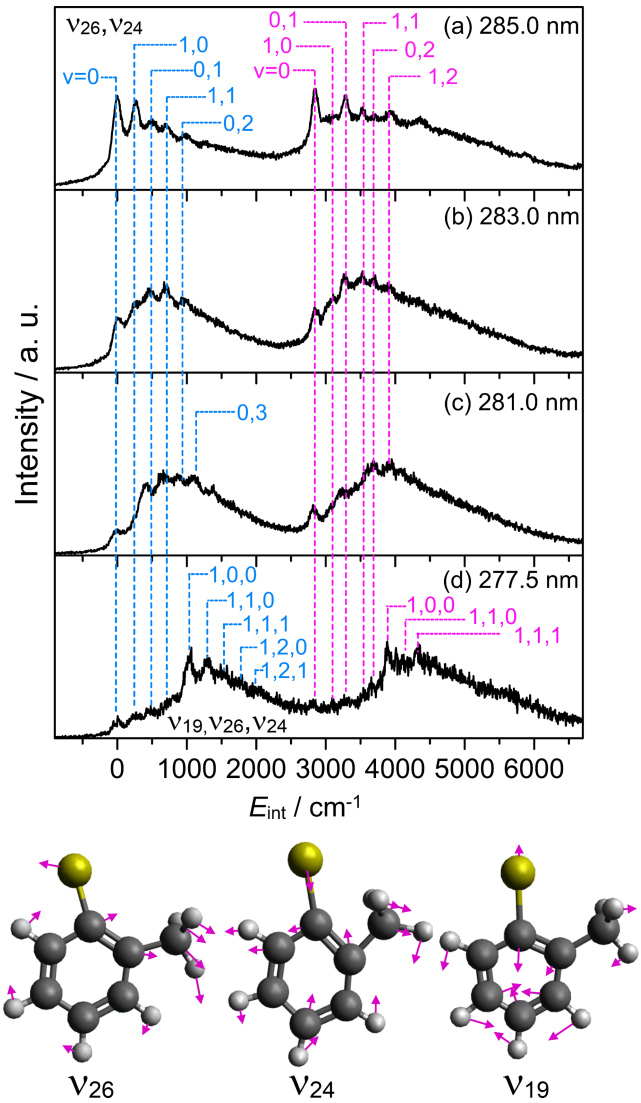


FIG. 5. $E_{int}$ spectra of the 2-MePhS radicals formed by photolysis of (predominantly) *anti*-2-MePhSH molecules at $\lambda_{phot}$ = (a) 285.0, (b) 283.0, (c) 281.0, and (d) 277.5 nm. Vibrational peak assignments for the $\tilde{X}$ and $\tilde{A}$ states of the radical are shown in blue and purple, respectively, along with the nuclear motions associated with the dominant active normal modes (below).

to the $1^1\pi\sigma^*$ continuum, prompt S–H bond fission, and preferential release of the excess energy as product translation.

$E_{int}$ spectra for the 3-MePhS fragments from photolysis of jet-cooled 3-MePhSH molecules are shown in Figure S1 of the supplementary material but, simply by inspecting the selection of TKER spectra shown in Figure 4, it is clear that the fragmentation dynamics, and their evolution with $\lambda_{phot}$, closely parallel that displayed by 2-MePhSH.

### 2. FPhSH

Figures 6 and 7 show, respectively, TKER spectra of the H + 3-FPhS products and selected $E_{int}$(3-FPhS) spectra derived therefrom following photoexcitation of jet-cooled 3-FPhSH molecules at various near UV wavelengths. These show clear similarities with the corresponding spectra obtained from photolysis of 2- and 3-MePhSH (above) and can be interpreted similarly. Again, the spectra show clear maxima attributable to the formation of $\tilde{X}$ and $\tilde{A}$ state radicals, and sufficient partially resolved vibrational structure to allow estimation of

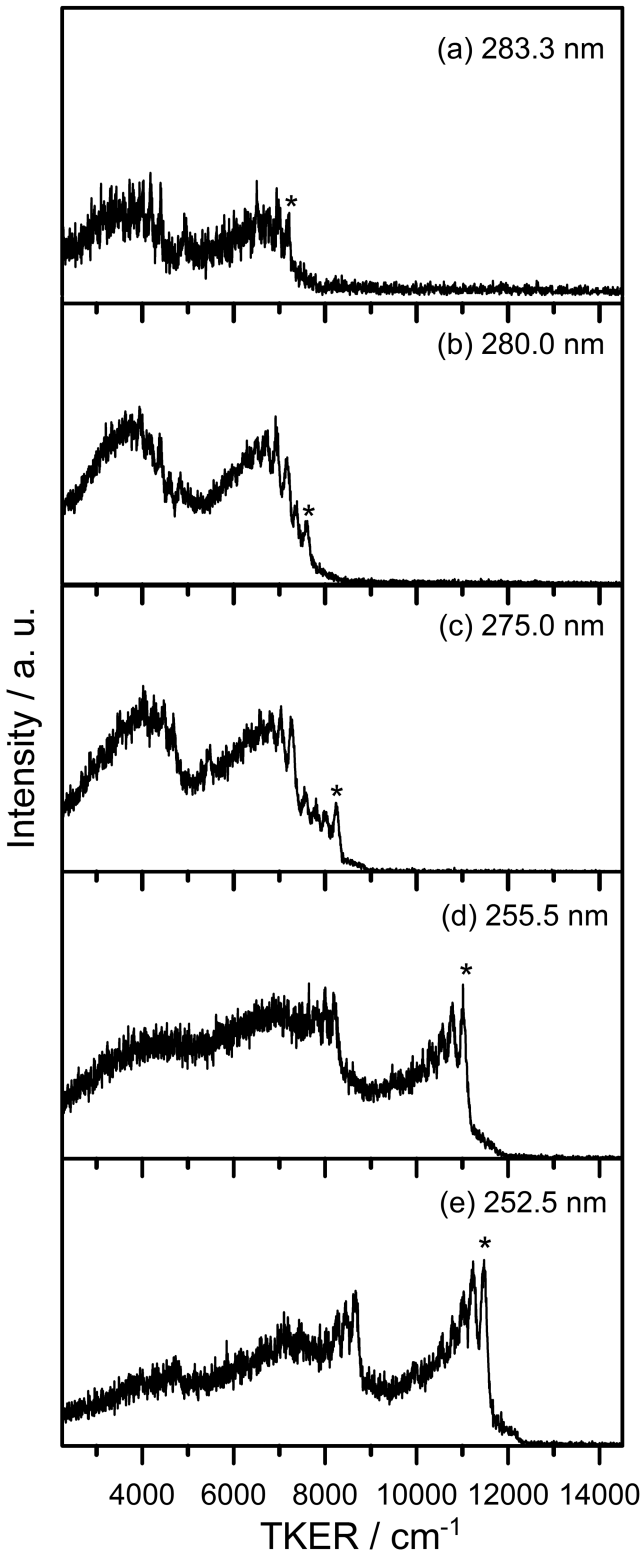


FIG. 6. TKER spectra of the H + 3-FPhS products derived by converting H atom TOF spectra measured following photolysis of 3-FPhSH at $\lambda_{phot}$ = (a) 283.3, (b) 280.0, (c) 275.0, (d) 255.5, and (e) 252.5 nm. In each spectrum, the $TKER_{max}$ peak attributed to the formation of H + 3-FPhS($\tilde{X}$), v = 0 products is indicated with an asterisk.

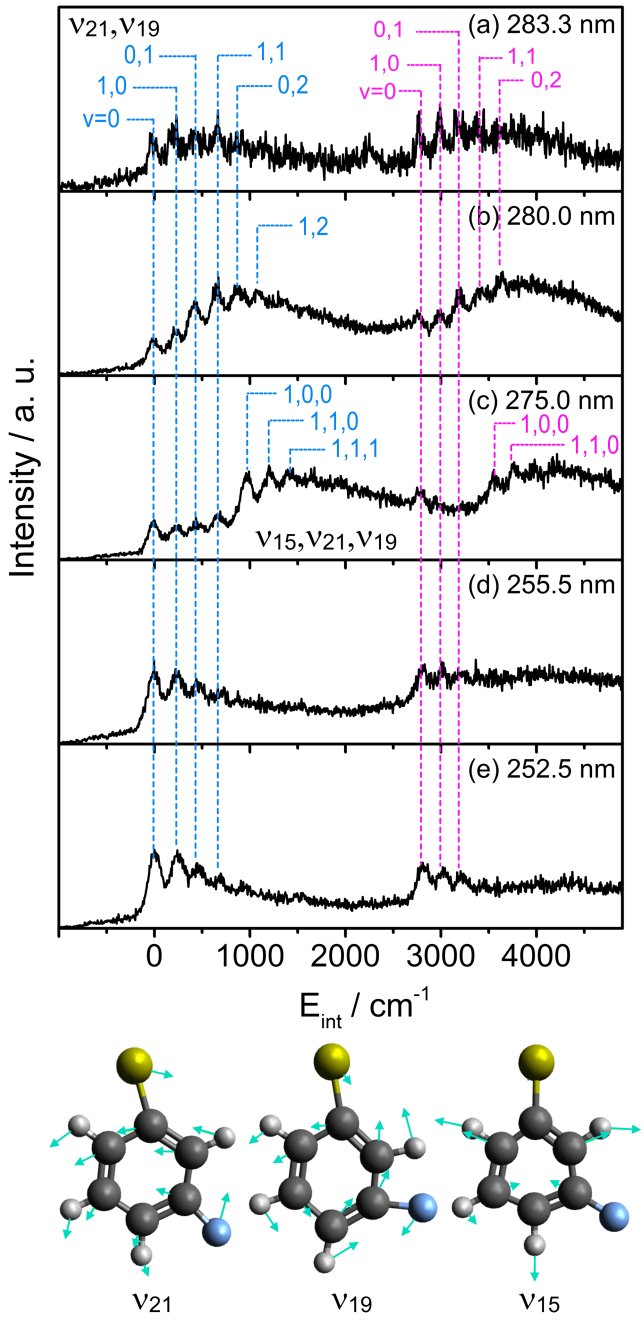


FIG. 7. $E_{int}$ spectra of the 3-FPhS radicals formed by photolysis of 3-FPhSH molecules at $\lambda_{phot}$ = (a) 283.3, (b) 280.0, (c) 275.0, (d) 255.5, and (e) 252.5 nm. Vibrational peak assignments for the $\tilde{X}$ and $\tilde{A}$ states of the radical are shown in blue and purple, respectively, along with the nuclear motions associated with the dominant active normal modes (below).

the S–H bond dissociation energy, $D_0$(R–H) = 28 130 ± 50 $cm^{-1}$, and the term value of the $\tilde{A}$ state radical: $\Delta E(\tilde{A}(v = 0) - \tilde{X}(v = 0)) = 2790 \pm 50\ cm^{-1}$. The resolution of this fine structure is consistent with the theoretical prediction that the *syn* and *anti* rotamers of this 3-substituted thiophenol are essentially degenerate. Reference to the calculated normal mode wavenumbers of the 3-FPhS radical (Table S1 of the supplementary material) highlights the similarity of the product vibrational energy disposal to that observed in the photolysis of 3-MePhSH. The $E_{int}$ spectrum measured at $\lambda_{phot}$ = 280 nm is most readily assigned in terms of short progressions in the C–S wag ($\nu_{21}$) and an in-plane ring breathing mode ($\nu_{19}$). The eigenvectors of both modes are shown in Figure 7. This pattern persists on tuning to shorter $\lambda_{phot}$ (275 nm) but is replicated at higher $E_{int}$. The offset wavenumber (~980 $cm^{-1}$) matches well with that of the in-plane ring breathing mode $\nu_{15}$ ($\nu_1$ in Wilson notation). As before, the

observed activity in this "spectator" product mode can be rationalised as a carry-over from population of the corresponding parent vibration in the initial photoexcitation process. Tuning to yet shorter $\lambda_{phot}$ (e.g., 255.5 nm) again results in an increased relative yield of vibrationally "cold" radicals, consistent with initial excitation to the $2^1\pi\pi^*$ state, rapid non-radiative transfer to the $1^1\pi\sigma^*$ continuum, and release of the excess energy as product translation.

2-FPhSH is different in several regards. Recalling Figure 2, it is the only one of the molecules studied in this work for which the 1+1 REMPI spectrum via the $1^1\pi\pi^*$ state shows a well-resolved vibronic structure. Han *et al.*[39] showed that this structure is specifically associated with the *syn* rotamer. Excitation at $\lambda_{phot}$ = 281.25 and 278.65 nm (resonances assigned to the $v = 0 \leftarrow v = 0$ origin band and the $v_{6a} = 1 \leftarrow v = 0$ transitions of this rotamer, with respective wavenumbers of 35 555 and 35 888 $cm^{-1}$) yields the structured TKER spectra shown in Figures 8(b) and 8(c). Spectra obtained when exciting at shorter $\lambda_{phot}$ (e.g., at 255.0 and 250.0 nm, Figures 8(d) and 8(e)) have a similar bimodal appearance, but show less (or no) sharp structure. These observations can be understood in terms of the increasing parent vibrational state density at higher excitation energies and the likelihood that both *syn* and *anti* rotamers are contributing to the dissociation yield. More surprisingly, H atoms were also detected when exciting at wavelengths longer than that of the *syn* origin band. The TKER spectrum obtained following excitation at $\lambda_{phot}$ = 284.0 nm (Figure 8(a)) is also bimodal, but weak and devoid of fine structure. Energy considerations require that these H atoms must arise from excitation of internally excited ($v > 0$) *syn*-2-FPhSH molecules or of the minority *anti* component within our jet-cooled sample. In what follows, we argue in favour of the latter explanation.

Figure 9 shows rigid-body PECs along $R_{S-H}$ calculated at the CASPT2(12/11)/aug(S)-AVTZ level for the $S_0$, $1^1\pi\pi^*$, and $1^1\pi\sigma^*$ states of the *syn* and *anti* rotamers of 2-FPhSH. The PECs for the higher energy *anti* rotamer (Figure 9(b)), in which the S–H bond points away from the F substituent, are very similar to those reported previously for PhSH[38] and for 3-FPhSH and 3- and 2-MePhSH (Figure S2 in the supplementary material). The $1^1\pi\sigma^*$ PEC is smoothly repulsive and intersects the $1^1\pi\pi^*$ PEC near its potential minimum. Any barrier under CI-1 is unlikely to offer much impediment to eventual S–H bond fission following $1^1\pi\pi^* \leftarrow S_0$ excitation. As Figure 9(a) shows, the situation in *syn*-2-FPhSH is rather different. Consistent with the earlier rigid-body calculations of Han *et al.*,[39] we find an obvious point of inflection in the $1^1\pi\sigma^*$ PEC that is likely attributable to Rydberg (4s)/valence ($\sigma^*$) mixing. The repulsive limb of the $1^1\pi\sigma^*$ PEC is shifted to a larger $R_{S-H}$, CI-1 is raised in energy, and the lifetimes of the lowest few levels within the $1^1\pi\pi^*$ potential well are sufficiently long that they support sharp features in the 1+1 REMPI spectrum (recall Figure 2(c)).

Armed with these PECs, we are now in a position to rationalise the TKER spectra reported in Figure 8. We start by considering the two $E_{int}$(2-FPhS) spectra derived from the TKER spectra shown in Figures 8(b) and 8(c). As Figures 10(a) and 10(b) show, features attributable to both $\tilde{X}$ and $\tilde{A}$ state radical products are again clearly evident, with near equal

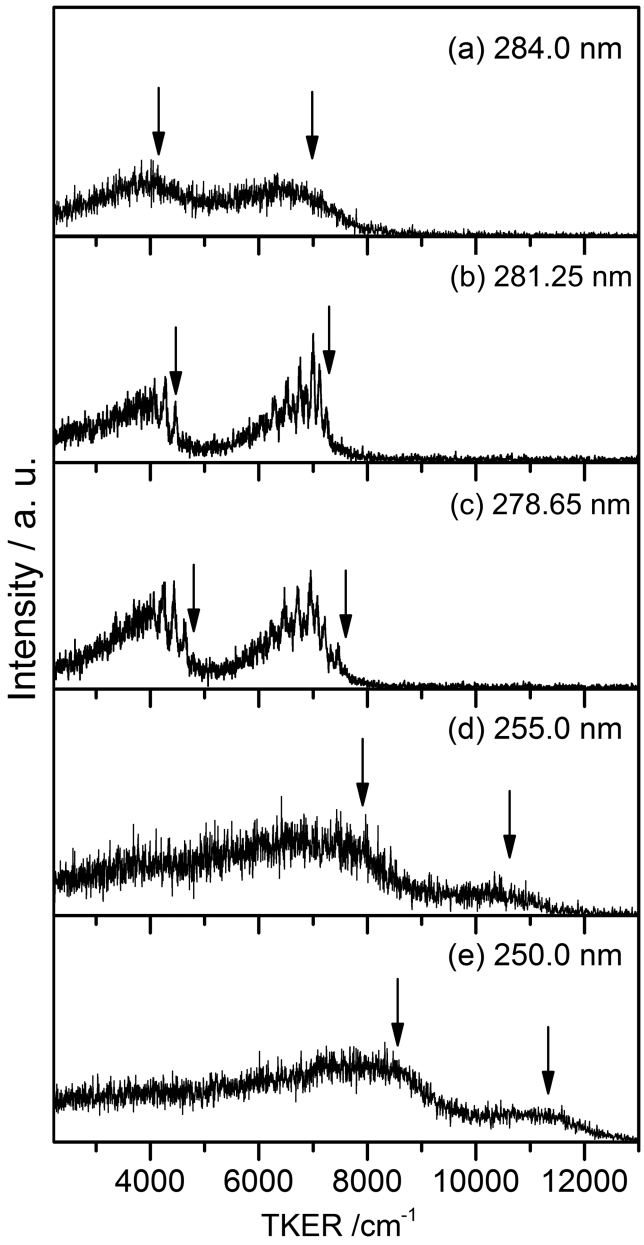


FIG. 8. TKER spectra of the H + 2-FPhS products derived by converting H atom TOF spectra measured following photolysis of 2-FPhSH at $\lambda_{phot}$ = (a) 284.0, (b) 281.25, (c) 278.65, (d) 255.0, and (e) 250.0 nm. The vertical arrows show the $TKER_{max}$ values expected for H + 2-FPhS($\tilde{X}/\tilde{A}$) products given the specified excitation wavelength and the values for $D_0$(*syn*-2-PhS–H) and the $\Delta E(\tilde{A}(v = 0) - \tilde{X}(v = 0))$ splitting in the 2-FPhS radical given in Table II.

yields—consistent with the findings of the earlier ion imaging study of the H atom products from 2-FPhSH photolysis at these same near UV wavelengths.[39] Both features in both spectra display an extended progression of peaks separated by ~240 $cm^{-1}$, with a weaker replica in the feature associated with $\tilde{X}$ state products offset by ~110 $cm^{-1}$. The 240 $cm^{-1}$ interval matches well with $\nu_{21}$, the in-plane C–S bending mode of the 2-FPhS radical. More extensive activity in this mode (cf. in the photodissociation of 2-MePhSH, for example) is plausible, given the evolving H-bonding with the adjacent F atom in the early stages of the S–H bond fission. As Table S1 of the supplementary material shows, no radical mode has a wavenumber as low as 110 $cm^{-1}$, but this value matches well with parent mode $\nu_{33}$, associated with the torsion of the

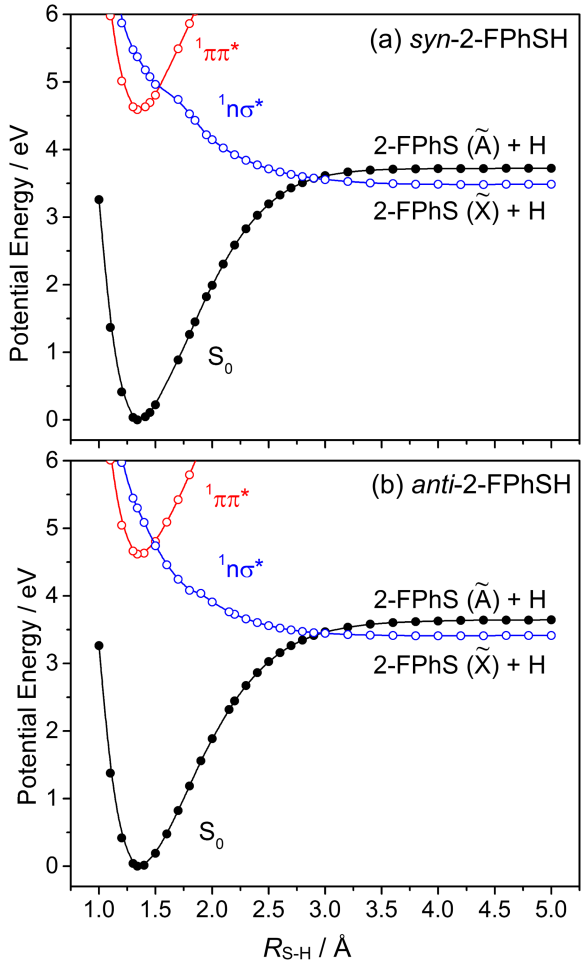


FIG. 9. PECs along $R_{S-H}$ for the $S_0$, $1^1\pi\pi^*$, and $1^1\pi\sigma^*$ states of the (a) *syn*- and (b) *anti* rotamers of 2-FPhSH calculated at the CASPT2/aug(S)-cc-pVTZ level, using the MP2 optimised $S_0$ geometries.

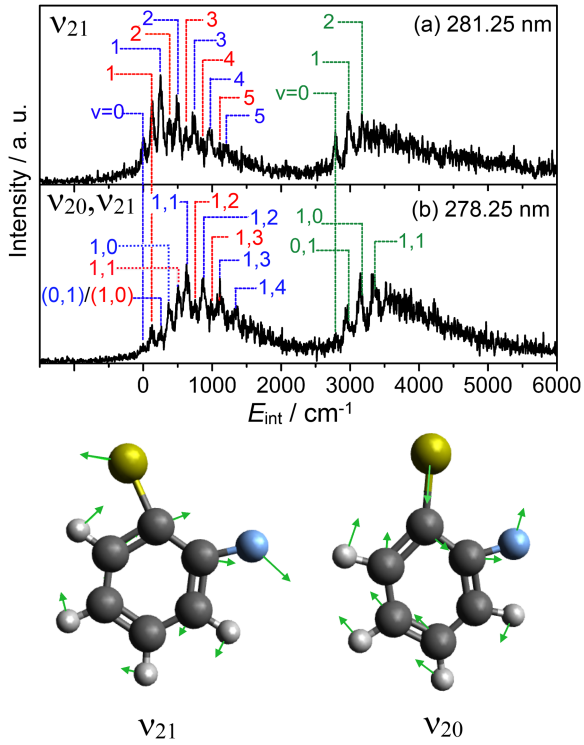


FIG. 10. $E_{int}$ spectra of the 2-FPhS radicals formed by photolysis of 2-FPhSH molecules at $\lambda_{phot}$ = (a) 281.25 nm and (b) 278.65 nm. Vibrational peak assignments for the $\tilde{X}$ and $\tilde{A}$ state radical products resulting from photolysis of *syn*-2-FPhSH(v = 0) molecules are shown in blue and green, respectively, along with the nuclear motions associated with the dominant active normal modes (below). The product peaks labelled in red are attributed to photoexcitation of *syn*-2-FPhSH($\nu_{33}$ = 1) molecules, and thus appear offset to lower $E_{int}$ because for these particular products $E_{int}$(RH) ~ 110 cm$^{-1}$ in Eq. (3).

S–H bond relative to the ring plane (i.e., with motion in the $\phi$ coordinate). It is thus tempting to assign the weaker replica progression to photodissociation of *syn*-2-FPhSH molecules in the $\nu_{33}$ = 1 level. 2-FPhS products in any given quantum state formed via such parent hot band excitation would appear in the TKER spectrum at a TKER value 110 cm$^{-1}$ higher than the corresponding products formed by exciting parent molecules in their v = 0 level, since the S–H torsional vibrational energy must be released as product translation upon S–H bond fission. Such products would thus appear in $E_{int}$ spectra such as those shown in Fig. 10 at $E_{int}$ values 110 cm$^{-1}$ lower than those formed from photodissociation of the corresponding *syn*-2-FPhSH(v = 0) molecules. Such an interpretation requires that the $\nu_{33}$ mode has a very similar wavenumber in the $S_0$ and $1^1\pi\pi^*$ states (as has been reported for the partially deuterated analogue 2-FPhSD[39]), i.e., that the $0_0^0$ origin band and $33_1^1$ hot band both contribute to the 2-FPhSH resonance excited at 35 555 cm$^{-1}$.

The peak assignments shown in Figure 10(a) are based on this interpretation and imply an S–H bond strength in *syn*-2-FPhSH of 28 310 ± 50 cm$^{-1}$. Excitation at 278.65 nm populates the $1^1\pi\pi^*$, $\nu_{6a}$ = 1 level[39] with a vibrational wavenumber of 333 cm$^{-1}$. The corresponding in-plane vibration in the $\tilde{X}$ state radical is $\nu_{20}$, with a calculated wavenumber of 390 cm$^{-1}$. As Figure 10(b) shows, the $E_{int}$ spectrum obtained at this wavelength is well described by assuming the same pattern of product vibrational energy disposal as when exciting on the origin band (and the overlapping hot band), but shifted by an amount equal to one quantum of the $\nu_{20}$ spectator mode.

The feature attributable to $\tilde{A}$ state radical products, in contrast, shows just one clear progression in radical mode $\nu_{21}$, hinting that the parent torsional excitation might affect the electronic branching in the radical products. In this regard, the recent study by Guo and co-workers[23] provides a possible rationale. This study describes the predissociation of $1^1\pi\pi^*$ state phenol molecules in terms of torsion-induced coupling to the corresponding $1^1\pi\sigma^*$ state in the region of CI-1. As in PhSH and the various substituted thiophenols, the $1^1\pi\pi^*$ and $1^1\pi\sigma^*$ states have A′ and A″ symmetries, respectively. Symmetry conservation thus requires that the $1^1\pi\pi^*$(v = 0) level couples to parent continuum states with $\nu_{33}$ = odd (i.e., levels of a″ vibrational symmetry, with a node in the wavefunction at $\phi$ = 0°). $1^1\pi\pi^*$ molecules prepared with $\nu_{33}$ = 1, in contrast, would couple to continuum states with $\nu_{33}$ = even (including 0), i.e., with a′ symmetry and maximal amplitude at $\phi$ = 0°. As noted in Section I, the electronic branching in the radical products is determined at CI-2, where molecules with $\phi$ ~ 0° are most likely to undergo non-adiabatic coupling (i.e., to follow the diabatic path) to $\tilde{X}$ state radical products. The simpler appearance of the $E_{int}$ feature associated with $\tilde{A}$ state radical products could thus be explained by assuming

that the $1^1\pi\pi^*(v_{33} = 1)$ molecules formed by unintended hot band excitation mainly dissociate to H + 2FPhS($\tilde{X}$) products. Such an interpretation, which implies $\Delta E(\tilde{A}(v = 0) - \tilde{X}(v = 0)) = 2780 \pm 50$ cm$^{-1}$, has been assumed in the $\tilde{A}$ state vibrational level assignments shown in Figure 10.

Little or no structure is evident in the other TKER spectra shown in Figure 8. The vertical arrows superposed above these spectra show the $TKER_{max}$ values expected for H + 2-FPhS($\tilde{X}/\tilde{A}$) products given the specified excitation wavelength and the values for $D_0$(*syn*-2-PhS–H) and the $\Delta E(\tilde{A}(v = 0) - \tilde{X}(v = 0))$ splitting in the 2-FPhS radical given in Table II. The spectrum in Figure 8(a) was obtained at a wavelength to the red of the $1^1\pi\pi^*$–$S_0$ origin of the *syn* rotamer, where no parent REMPI signal was observed. The spectrum extends to TKER values above that predicted following excitation and dissociation of *syn*-2-PhSH molecules and shows no obvious discontinuity around this predicted $TKER_{max}$ value. The most plausible source of the H atoms observed at this long wavelength is direct excitation of the minority population of the higher energy *anti* rotamer to heavily predissociated levels of its $1^1\pi\pi^*$ state or, more probably given the relative lowering of the potential (Figure 9(b)), directly to its $1^1\pi\sigma^*$ state. The TKER spectra measured at significantly shorter wavelengths are similarly lacking in fine structure, most probably because we are now exciting both *syn* and *anti* rotamers.

### D. Substituent effects

As in a previous combined experimental and theoretical study of how substituents affect O–H bond fission following photoexcitation to the $1^1\pi\pi^*$ state in a range of 4-substituted phenols,[34] we start by noting the similarity of the diabatic $S_0$ PECs along $R_{S-H}$ for each of the thiophenols listed in Table II. These diabatic potentials dissociate to the corresponding H + R($\tilde{A}$) radicals, so the well-depths of interest are the $D'$(R–H) values obtained by summing the (experimental) $D_0(R$–H) and $\Delta E(\tilde{A} - \tilde{X})$ values given in Table II. These all lie within the narrow range $D'$(R–H) = 30 670 cm$^{-1}$ (in the case of 2-MePhSH) to 31 110 cm$^{-1}$ (2-FPhSH) and straddle the value for bare thiophenol ($D'$(PhS–H) = 31 030 cm$^{-1}$). This narrow spread of values can be understood by recognizing that substituents will mainly influence the π-system and thus have little effect on the bonding interaction between the R($\tilde{A}$) radical (wherein the SOMO is the S($3p_y$) orbital orthogonal to the π-system) and the H(1s) atom. By this same logic, we can also anticipate that π-perturbing substituents will have a relatively greater effect on the energetics of the R($\tilde{X}$) state (the SOMO for which involves a major contribution from the S($3p_x$) orbital).

We now test the present data against such expectations, starting with 2-, 3-, and 4-FPhSH, for which the respective $D'$(R–H) values are 31 090, 30 920, and 30 840 cm$^{-1}$. The latter two values are the same within the combined uncertainties associated with each value. The larger $D'$(R–H) value for 2-FPhSH reflects the small additional stabilisation provided by the intramolecular H-bond in the *syn* rotamer. Adopting the calculated energy separation between the *syn* and *anti* rotamers (~280 cm$^{-1}$, Figure 1) gives $D'$(R–H) = 30 810 cm$^{-1}$ for the non-H-bonded *anti* rotamer—in close accord with the diabatic $S_0$ well depth for the 4-FPhSH isomer.

However, as Table II shows, the position of the F substituent does affect the $D_0$(R–H) and $\Delta E(\tilde{A} - \tilde{X})$ values. π-donating substituents like SH (and F) direct π-electron density to the 2- and 4-positions of the ring. The lower $D_0(R$–H) value found for 4-FPhSH and the concomitant increase in the $\Delta E(\tilde{A} - \tilde{X})$ value for the 4-FPhS radical are both fully consistent with such a picture. The π-donating F atom stabilises the electron deficient SOMO of the 4-FPhS($\tilde{X}$) radical and thereby lowers the asymptotic limit for forming 4-FPhS ($\tilde{X}$) + H products (relative to that found for bare PhSH, or for 3-FPhSH, where the F atom would be predicted to have least influence on the π-system of the parent or the resulting radical). From the foregoing, we might expect a similar reduction in $D_0(R$–H) and increase in $\Delta E(\tilde{A} - \tilde{X})$ in the case of 2-FPhSH. As noted above, the intramolecular H-bond in the ground state parent molecule is one contributor to the increase in the measured $D_0$(2-FPhS–H) value (cf. $D_0$(4-FPhS–H)). The FPhS radical is not affected by such effects, however, yet $\Delta E(\tilde{A} - \tilde{X})$ is found to be significantly smaller in 2-FPhS than in 4-FPhS. This can be rationalised if the expected stabilisation of the 2-FPhS($\tilde{X}$) radical by π-donation from the F atom is offset by an increase in electron repulsion between the doubly occupied $p_y$ valence orbitals of the S and F atoms. The calculated minimum energy geometry of the ground state radical is consistent with such expectations, e.g., the calculated ∠SC(1)C(2) bond angle in 2-FPhS is 122.4° (cf. 120.5°in 3-FPhS). Thus, the $\Delta E(\tilde{A} - \tilde{X})$ values for the 2-FPhS and 3-FPhS radicals are very similar and, given the near constancy of $D'$(R–H), the $D_0$(R–H) values for (the non-H-bonded *anti*-rotamer of) 2-FPhSH and for 3-FPhSH are necessarily also the same (to within experimental uncertainty).

The Me group is generally viewed as a σ-perturbing substituent, so we should expect—and indeed observe—less variation in the S–H bond strengths in the various positional isomers of MePhSH. The respective $D'$(R–H) values for 2-, 3-, and 4-MePhSH are 30 670, 30 840, and 30 750 cm$^{-1}$. All are similar to, but consistently slightly smaller than, that for bare PhSH. The mild softening of the S–H bond in all three isomers is consistent with Me acting as a weak electron donor (+I inductive effect). Further interpretation requires caution, given that the differences between these $D'$(R–H) values are no bigger than the combined uncertainties associated with each value. Nonetheless, the finding that the (*anti* rotamer) of 2-MePhSH shows the lowest $D'$(R–H) value would be consistent with some weak destabilisation of the in-plane sulfur $3p_y$ electron by the proximal Me group. More definitively, the $\Delta E(\tilde{A} - \tilde{X})$ values are found (experimentally and by computation) to increase in the order 2- < 3- < 4-MePhS. Given the relative constancy of the $D'$(R–H) values, this trend must primarily reflect changes in the relative stability of the $\tilde{X}$ state radicals. The observed trends can be understood by invoking a larger destabilisation of the (now doubly occupied) in-plane sulfur $3p_y$ electron in the case of 2-MePhS and stabilisation (by hyperconjugation) of the electron deficient π-system in the case of 4-MePhS.

## IV. CONCLUSIONS

Previous studies of ways in which ring-substituents affect the dynamics and energetics of photoinduced O–H

bond fission in phenols[16,17,31–36] and S–H bond fission in thiophenols[37–39] have been extended to the cases of 2- and 3-YPhSH (with Y = Me and F). Using a combination of experiment—H (Rydberg) atom PTS, at many different near UV excitation wavelengths—and complementary electronic structure methods, we have been able to gain further insights into the interplay between substituent-induced geometric (i.e., steric effect/intramolecular hydrogen bonding) and electronic (i.e., π (resonance) or σ (inductive)) effects. Theory shows that the *syn* and *anti* rotamers of the 3-YPhSH species are essentially degenerate, but returns much larger rotamer splittings in the 2-YPhSH isomers. In the case of 2-FPhSH, intramolecular H-bonding between the SH hydrogen and the adjacent F atom ensures that the ground state molecule adopts the *syn* geometry, whilst destabilising steric interactions between the SH hydrogen and the adjacent Me group ensures that the *anti* rotamer is the more stable form of 2-MePhSH. Near UV photolysis of all four molecules, at all wavelengths investigated, yields the corresponding 2-(3-)YPhS radical in both its ground ($\tilde{X}$) and first excited ($\tilde{A}$) electronic states. For all species investigated, one or more of the measured TKER spectra revealed sufficient structure to allow determination of the S–H bond strength, $D_0$(R–H), the energy separation between the $\tilde{A}$ and $\tilde{X}$ states of the radical, $\Delta E(\tilde{A}-\tilde{X})$, and identification of vibrational modes that are preferentially populated in the radical photoproducts.

Ring substituents, even in the 2-position, are found to have rather little influence on the depth of the diabatic $S_0$ potential, $D'$(R–H) (i.e., the binding energy measured relative to the R($\tilde{A}$) + H asymptote), but relatively greater impact on the adiabatic well depth, $D_0$(R–H), and the $\Delta E(\tilde{A}-\tilde{X})$ splitting. The observed differences are primarily due to the stabilising (destabilising) influence that the substituent has on the $\tilde{X}$ state of the radical. An F atom (a π-donor) stabilises the electron deficient SOMO of the 4-FPhS($\tilde{X}$) radical and thereby lowers $D_0$(R–H) in the case of 4-FPhSH (cf. the corresponding S–H bond strengths in bare PhSH or 3-FPhSH). The corresponding resonance stabilisation that might have been expected in the case of the 2-FPhS($\tilde{X}$) radical appears to be offset by a destabilising interference between the singly occupied in-plane sulfur $3p_y$ orbital and the adjacent F atom. Relative to an F atom, a Me radical is generally viewed as a milder perturber, but the deduced $\Delta E(\tilde{A}-\tilde{X})$ values clearly increase in the order 2- < 3- < 4-MePhS. The $\Delta E(\tilde{A}-\tilde{X})$ value for 3-MePhS is sensibly consistent with that for the PhS radical itself. The reduced splitting in the 2-MePhS radical reflects a destabilisating interaction between the (doubly occupied) $3p_y$ orbital on the S atom and the adjacent Me group, while the increased $\Delta E(\tilde{A}-\tilde{X})$ value for 4-MePhS can be attributed to hyperconjugative stabilisation of the SOMO in the ground state radical by the Me group.

The deduced fragmentation dynamics and the energy disposal in the radical products show obvious parallels with that found in previous photolysis studies of PhSH[26] and various 4-substituted thiophenols.[38] Long wavelength excitation of 2- and 3-MePhSH, and of 3-FPhSH, populates the $1^1\pi\sigma^*$ state (either directly or by efficient coupling from the $1^1\pi\pi^*$ state) which subsequently undergoes prompt S–H bond fission to yield radical fragments in both the $\tilde{X}$ and $\tilde{A}$ electronic states in a range of vibrational states. Analysis of structure evident in the TKER spectra reveals obvious propensities for exciting the C–S in-plane bending mode in the radical product along with various different in-plane ring breathing modes. The activation of such motions is unsurprising, given the changes in the π electron density induced by the initial photoexcitation step and in the subsequent evolution from excited state parent to radical product.

2-FPhSH shows some obvious but subtle spectroscopic and photochemical differences. The intramolecular H-bond ensures that most 2-FPhSH molecules are present as the *syn* rotamer, for which the present (and previous[39]) rigid body electronic structure calculations suggest a much greater impediment to tunnelling from the photoexcited $1^1\pi\pi^*$ state through the barrier under CI-1. Thus, in contrast to all the other substituted thiophenols studied in this work, the $1^1\pi\pi^*\leftarrow S_0$ excitation spectrum for the *syn* rotamer of 2-FPhSH exhibits well resolved vibronic structure, enabling photolysis studies with a higher level of parent state selectivity. Unsurprisingly, the TKER spectrum obtained when exciting on the $1^1\pi\pi^* \leftarrow S_0$ origin band reveals population of vibrationally excited levels of the C–S in-plane bending mode of the 2-FPhS radical products (i.e., the analogous motion to that identified in the products formed when photolysing the other thiophenols). The $E_{int}$ spectrum of the 2-FPhS($\tilde{X}$) products, in particular, is unexpectedly structured, however. The spectrum is most logically interpreted by assuming unintended photoexcitation of an overlapping resonance associated with *syn*-2-FPhSH($\nu_{33}$ = 1) molecules. Parent mode $\nu_{33}$ is a low frequency, out-of-plane torsional motion, and the present data provide tantalising hints in support of recent theoretical predictions[23,28,29] that such out-of-plane motions in molecules of this type should influence the non-adiabatic coupling in the vicinity of CI-2 and the eventual electronic branching in the radical products.

## SUPPLEMENTARY MATERIAL

See supplementary material for (i) DFT/B3LYP/6-311G(d,p)++ normal mode wavenumbers (in $cm^{-1}$) for the ground states for 3-MePhS, 2-MePhS, 3-FPhS, and 2-FPhS computed with anharmonic correction and numbered following Herzberg notation; (ii) internal energy ($E_{int}$) spectra of the 3-MePhS radicals formed by UV photolysis of jet-cooled 3-MePhSH molecules following photolysis at $\lambda_{phot}$ = (a) 290.0, (b) 271.7, (c) 255.0, and (d) 250.0 nm, with vibrational peak assignments for both the $\tilde{X}$ and $\tilde{A}$ states of the 3-MePhS radical and depictions of the nuclear motions associated with the dominant active normal modes; (iii) PECs along $R_{S-H}$ for the $S_0$, $1^1\pi\pi^*$, and $1^1\pi\sigma^*$ states of (a) *anti*-2-MePhSH, (b) *syn*-3-MePhSH, and (c) *syn*-3-FPhSH calculated at the CASPT2/aug(S)-AVTZ level of theory, using the MP2 optimised $S_0$ geometries.

## ACKNOWLEDGMENTS

The authors acknowledge financial support from the Engineering and Physical Sciences Research Council (EPSRC), Programme Grant No. EP/L005913/1. B.M. and T.N.V.K. are also both grateful to T. U. München for the award of

post-doctoral research fellowships during the tenure of which much of the present analysis was undertaken. Raw data used in the preparation of this paper have been placed in the University of Bristol's research data repository and can be accessed at http://dx.doi.org/10.5523/bris.3i6yzrcdzlpwj268bqtcluzo2s.


[1] A. L. Sobolewski and W. Domcke, Chem. Phys. **259**, 181 (2000).
[2] A. L. Sobolewski, W. Domcke, C. Dedonder-Lardeux, and C. Jouvet, Phys. Chem. Chem. Phys. **4**, 1093 (2002).
[3] M. N. R. Ashfold, B. Cronin, A. L. Devine, R. N. Dixon, and M. G. D. Nix, Science **312**, 1637 (2006).
[4] M. N. R. Ashfold, A. L. Devine, R. N. Dixon, G. A. King, M. G. D. Nix, and T. A. A. Oliver, Proc. Natl. Acad. Sci. U. S. A. **105**, 12701 (2008).
[5] M. N. R. Ashfold, G. A. King, D. Murdock, M. G. D. Nix, T. A. A. Oliver, and A. G. Sage, Phys. Chem. Chem. Phys. **12**, 1218 (2010).
[6] G. M. Roberts and V. G. Stavros, Chem. Sci. **5**, 1698 (2014).
[7] H. S. You, S. Han, J.-H. Yoon, J. S. Lim, J. Lee, S. Y. Kim, D.-S. Ahn, J. S. Lim, and S. K. Kim, Int. Rev. Phys. Chem. **34**, 429 (2015).
[8] C.-M. Tseng, Y. T. Lee, and C.-K. Ni, J. Chem. Phys. **121**, 2459 (2004).
[9] M. G. D. Nix, A. L. Devine, B. Cronin, R. N. Dixon, and M. N. R. Ashfold, J. Chem. Phys. **125**, 133318 (2006).
[10] C. M. Tseng, Y. T. Lee, C.-K. Ni, and J. L. Chang, J. Phys. Chem. A **111**, 6674 (2007).
[11] C. M. Tseng, Y. T. Lee, M. F. Lin, C.-K. Ni,S. Y. Liu, Y. P. Lee, Z. F. Xu, and M. C. Lin, J. Phys. Chem. A **111**, 9463 (2007).
[12] A. Iqbal, L. J. Pegg, and V. G. Stavros, J. Phys. Chem. A **112**, 9531 (2008).
[13] O. P. J. Vieuxmaire, Z. Lan, A. L. Sobolewski, and W. Domcke, J. Chem. Phys. **129**, 224307 (2008).
[14] G. A. King, T. A. A. Oliver, M. G. D. Nix, and M. N. R. Ashfold, J. Phys. Chem. A **113**, 7984 (2009).
[15] A. Iqbal, M. S. Y. Cheung, M. G. D. Nix, and V. G. Stavros, J. Phys. Chem. A **113**, 8157 (2009).
[16] G. A. Pino, A. N. Oldani, E. Marceca, M. Fujii, S. I. Ichiuchi, M. Miyazaki, M. Broquier, C. Dedonder, and C. Jouvet, J. Chem. Phys. **133**, 124313 (2010).
[17] R. N. Dixon, T. A. A. Oliver, and M. N. R. Ashfold, J. Chem. Phys. **134**, 194303 (2011).
[18] G. M. Roberts, A. S. Chatterley, J. D. Young, and V. G. Stavros, J. Phys. Chem. Lett. **3**, 348 (2012).
[19] S. G. Ramesh and W. Domcke, Faraday Discuss. **163**,73 (2013).
[20] X. F. Xu, K. R. Yang, and D. G. Truhlar, J. Chem. Theory Comput. **9**, 3612 (2013).
[21] K. R. Yang, X. F. Xu, J. J. Zheng, and D. G. Truhlar, Chem. Sci. **5**, 4661 (2014).
[22] X. F. Xu, J. J. Zheng, K. R. Yang, and D. G. Truhlar, J. Am. Chem. Soc. **136**, 16378 (2014).
[23] C. J. Xie, J. Y. Ma, X. L. Zhu, D. R. Yarkony, D. Q. Xie, and H. Guo, J. Am. Chem. Soc. **138**, 7828 (2016).
[24] J. S. Lim, I. S. Lim, K.-S. Lee, D.-S. Ahn, Y. S. Lee, and S. K. Kim, Angew. Chem., Int. Ed. **45**, 6290 (2006).
[25] I. S. Lim, J. S. Lim, Y. S. Lee, and S. K. Kim, J. Chem. Phys. **126**, 034306 (2007).
[26] A. L. Devine, M. G. D. Nix, R. N. Dixon, and M. N. R. Ashfold, J. Phys. Chem. A **112**, 9563 (2008).
[27] J. S. Lim, H. Choi, I. S. Lim, S. B. Park, Y. S. Lee, and S. K. Kim, J. Phys. Chem. A **113**, 10410 (2009).
[28] T. S. Venkatesan, S. G. Ramesh, Z. Lan, and W. Domcke, J. Chem. Phys. **136**, 174312 (2012).
[29] H. An, H. Choi, Y. S. Lee, and K. K. Baeck, ChemPhysChem **16**, 1529 (2015).
[30] H. S. You, S. Han, J. S. Lim, and S. K. Kim, J. Phys. Chem. Lett. **6**, 3202 (2015).
[31] A. L. Devine, M. G. D. Nix, B. Cronin, and M. N. R. Ashfold, Phys. Chem. Chem. Phys. **9**, 3749 (2007).
[32] G. A. King, A. L. Devine, M. G. D. Nix, D. E. Kelly, and M. N. R. Ashfold, Phys. Chem. Chem. Phys. **10**, 6417 (2008).
[33] A. G. Sage, T. A. A. Oliver, G. A. King, D. Murdock, J. N. Harvey, and M. N. R. Ashfold, J. Chem. Phys. **138**, 164318 (2013).
[34] T. N. V. Karsili, A. M. Wenge, D. Murdock, S. J. Harris, J. N. Harvey, R. N. Dixon, and M. N. R. Ashfold, Chem. Sci. **4**, 2434 (2013).
[35] T. N. V. Karsili, A. M. Wenge, B. Marchetti, and M. N. R. Ashfold, Phys. Chem. Chem. Phys. **16**, 588 (2014).
[36] S. J. Harris, T. N. V. Karsili, D. Murdock, T. A. A. Oliver, A. M. Wenge, D. K. Zaouris, M. N. R. Ashfold, J. N. Harvey, J. D. Few, S. Gowrie, G. Hancock, D. J. Hadden, G. M. Roberts, V. G. Stavros, G. Spighi, L. Poisson, and B. Soep, J. Phys. Chem. A **119**, 6045 (2015).
[37] J. S. Lim, Y. S. Lee, and S. K. Kim, Angew. Chem., Int. Ed. **47**, 1853 (2008).
[38] T. A. A. Oliver, G. A. King, D. P. Tew, R. N. Dixon, and M. N. R. Ashfold, J. Phys. Chem. A **116**, 12444 (2012).
[39] S. Han, Y. S. Hou, S. Y. Kim, and S. K. Kim, J. Phys. Chem. A **118**, 6940 (2014).
[40] C. M. Tseng, Y. T. Lee, and C.-K. Ni, J. Phys. Chem. A **113**, 3881 (2009).
[41] D. J. Hadden, C. A. Williams, G. M. Roberts, and V. G. Stavros, Phys. Chem. Chem. Phys. **13**, 4494 (2011).
[42] G. M. Roberts, D. J. Hadden, L. T. Bergendahl, A. M. Wenge, S. J. Harris, T. N. V. Karsili, M. N. R. Ashfold, M. J. Paterson, and V. G. Stavros, Chem. Sci. **4**, 993 (2013).
[43] S. H. L. Li, X. F. Xu, C. E. Hoyer, and D. G. Truhlar, J. Phys. Chem. Lett. **6**, 3352 (2015).
[44] S. H. L. Li, X. F. Xu, and D. G. Truhlar, Phys. Chem. Chem. Phys. **17**, 20093 (2015).
[45] S.-Y. Kim, J. Lee, S. K. Kim, and Y. S. Choi, Chem. Phys. Lett. **659**, 43 (2016).
[46] S. L. Li and D. G. Truhlar, J. Chem. Phys. **146**, 064301 (2017).
[47] T. A. A. Oliver, Y. Zhang, M. N. R. Ashfold, and S. E. Bradforth, Faraday Discuss. **150**, 439 (2011).
[48] Y. Zhang, T. A. A. Oliver, M. N. R. Ashfold, and S. E. Bradforth, Faraday Discuss. **157**, 141 (2012).
[49] D. Murdock, S. J. Harris, T. N. V. Karsili, G. M. Greetham, I. P. Clark, M. Towrie, A. J. Orr-Ewing, and M. N. R. Ashfold, J. Phys. Chem. Lett. **3**, 3715 (2012).
[50] Y. Zhang, T. A. A. Oliver, S. Das, A. Roy, M. N. R. Ashfold, and S. E. Bradforth, J. Phys. Chem. A **117**, 12125 (2013).
[51] R. A. Ingle, T. N. V. Karsili, G. J. Dennis, M. Staniforth, V. G. Stavros, and M. N. R. Ashfold, Phys. Chem. Chem. Phys. **18**, 11401 (2016).
[52] H.-J. Werner, P. J. Knowles, G. Knizia, F. R. Manby, M. Schütz *et al.*, MOLPRO, version 2010.1, a package of *ab initio* programs, 2010, see http://www.molpro.net.
[53] T. Dunning, Jr., J. Chem. Phys. **90**, 1007 (1989).
[54] H. Koch and P. Jørgensen, J. Chem. Phys. **93**, 3333 (1990).
[55] A. D. Becke, J. Chem. Phys. **98**, 5648 (1993).
[56] R. Krishnan, J. S. Binkley, R. Seeger, and J. A. Pople, J. Chem. Phys. **72**, 650 (1980).
[57] M. J. Frisch, G. W. Trucks, H. B. Schlegel *et al.*, GAUSSIAN 09, Revision B.01, Gaussian, Inc., Wallingford, CT, 2009.
[58] J. B. Kim, T. I. Yacovich, C. Hock, and D. M. Neumark, Phys. Chem. Chem. Phys. **13**, 17378 (2011).
[59] G. Herzberg, *Molecular Spectra and Molecular Structure II. Infrared and Raman Spectra of Polyatomic Molecules* (Van Nostrand Reinhold, New York, 1945).
[60] E. B. Wilson, Phys. Rev. **45**, 706 (1934).